Research Square

Preprints are preliminary reports that have not undergone peer review.
They should not be considered conclusive, used to inform clinical practice,
or referenced by the media as validated information.

Mechanosensing Piezo1 mediates gut-vascular barrier dysfunction in portal hypertension and promotes deterioration of liver cirrhosis

Lei Zhang

zhanglei2017@hust.edu.cn

Wuhan Union Hospital

Zhuanglong Xiao

Wuhan Union Hospital

Jun Song

Union Hospital, Tongji Medical College Medical College, Huazhong University of Science and Technology

Jing He

Wuhan Union Hospital

Wenjing Tian

Wuhan Union Hospital

li Du

Wuhan Union Hospital

Ruiyun Wang

Wuhan Union Hospital

Tao Bai

Union Hospital, Tongji Medical College, Huazhong University of Science and Technology

Wei Qian

Wuhan union hospital

Xiaohua Hou

Wuhan Union Hospital

Article

Keywords: Piezo1, Endothelial cells, Gut-vascular barrier, Portal hypertension, Liver cirrhosis

Posted Date: May 15th, 2026

DOI: https://doi.org/10.21203/rs.3.rs-9418908/v1

License: This work is licensed under a Creative Commons Attribution 4.0 International License.
Read Full License

Additional Declarations: There is no conflict of interest

Abstract

Objectives

Gut-vascular barrier (GVB) disruption in cirrhotic portal hypertension (PH) exacerbates hepatic and systemic damage via the gut-liver-organ axis, but the underlying mechanism is unclear. The mechanosensitive channel Piezo1, known to regulate endothelial homeostasis, may mediate GVB dysfunction, requiring validation.

Methods

Carbon tetrachloride (CCl_4)-induced liver cirrhosis and partial portal vein ligation (PPVL)-induced pre-hepatic PH model were established in Piezo1$^{flox/flox}$ and endothelial cells (ECs)-specific Piezo1-deficient (Piezo1$^{\triangle EC}$) mice. Portal pressure, GVB permeability, intestinal and systemic inflammation, and Piezo1 expression in mucosal ECs were measured. Cultured intestinal microvascular ECs were treated with the Piezo1 agonist Yoda1 or hydrostatic pressure to investigate Piezo1-mediated endothelial barrier regulation.

Results

PH induced significant GVB breakdown in CCl_4 and PPVL mice, presented as increased permeability from the gut-to-blood and also leakage from blood-to-gut, accompanied by increased Piezo1 and VEGFR2 expression in ECs, along with systemic and intestinal inflammation and leaky epithelium. These effects were reversed in Piezo1$^{\triangle EC}$ mice, and Piezo1 knockout in ECs reduced VEGFR2 expression which in turn inhibited intestinal leakage and inflammatory infiltration, and meanwhile improved systemic inflammation. Moreover, Yoda1 or hydrostatic pressure promoted VEGFR2 phosphorylation and ECs monolayer disruption, blocked by siRNA of *Piezo1* or *Vegfr2*.

Conclusion

Endothelial Piezo1 contributed to GVB dysfunction in PH via VEGFR2 pathway. The outward and inward hyper-permeability of GVB in PH may initiate the intestinal inflammation and trigger epithelial leakage, and further cause systemic inflammation and injury. Therefore, Piezo1-mediated GVB damage may be a novel explanation and potential therapeutic target for deterioration of liver cirrhosis with PH.

INTRODUCTION

Cirrhosis, the end stage of chronic liver disease caused by various reasons(1), is a major global health concern with high morbidity and mortality rates worldwide(2). Portal hypertension (PH) and declined liver function are the main features of progressive cirrhosis(3). In particular, patients with cirrhosis are susceptible to microbiota translocation and entry of enterogenous toxins into the bloodstream, which may trigger systemic inflammation and injury(4). These bacterial infections promote the progression and

decompensation of cirrhosis, in some cases, can lead to life-threatening acute-on-chronic liver failure and even multi-organ failure via the gut-liver-organ axes(5–7). Currently, targeting the gut-liver axis has become an important strategy and viewpoint for preventing further liver damage and related multi-organ injury in cirrhosis.

Intestinal mucosal barrier dysfunction is commonly found in chronic liver disease and cirrhosis(8), with destroyed integrity of mucus layer and capability of immune defense, and increased epithelial permeability(9). Recently, beneath the epithelial barrier, a newly gut-vascular barrier (GVB) was characterized and proved important role in liver injury(9–11), which is the structural and functional unit formed by microvascular endothelial cells (ECs), pericytes and enteric glial cells (Figure S1)(12, 13). GVB acts as the last key guard between the intestine and liver, as well as the blood circulation, it defends against the dissemination of bacteria and luminal antigen that escaped from the epithelial barrier(14, 15). Most of the invaded pathogens from the intestinal epithelium are denied entry to the internal environment by GVB, and are finally phagocytose and clear by macrophages and other immunocytes(13). Indubitably, GVB disruption may directly result in liver injury, and was confirmed in various intestinal inflammatory conditions(15) and hepatic diseases, such as metabolic associated fatty liver disease (MAFLD), alcoholic liver disease (ALD) and cirrhosis(11, 16, 17). However, the specific target and mechanism underlying GVB collapse is far from clear.

Liver cirrhosis may disrupt the intestinal barrier integrity through gut dysbiosis and abnormal bile acid metabolism in enterohepatic circulation as reported in previous studies(18, 19). Even so, the direct mechanisms of liver cirrhosis on intestinal barrier, especially for the GVB, are still largely unclear. It is well-known that PH can cause direct damage to the gastrointestinal tract, so called portal hypertensive enteropathy(20). The intestinal microvascular ECs may bear the first brunt from PH-induced rise of intravessel pressure and blood stasis, which is speculated to bring about GVB collapse, and intestinal edema and inflammation. To date, little is known about vascular mechanical sensing in inducing endothelial barrier disruption.

Piezo1, a mechanosensitive ion channel expressed in ECs, is activated by elevated pressure and other mechanical stimuli(21). Piezo1 was proven to play a crucial role in the endothelial homeostasis and angiogenesis, such as pulmonary artery(22, 23), coronary artery(24), brain capillary(25–27) and intestinal microvessel(28). Piezo1 could sense disturbed blood flow and activated endothelial inflammatory signaling(29, 30). Upregulation of Piezo1 in ECs leads to vascular remodeling and pulmonary hypertension induced by high shear stress(23). In particular, endothelial Piezo1 mediated pressure-induced lung vascular hyper-permeability via disruption of adherens junctions, while inhibition or deletion of Piezo1 in ECs markedly prevented capillary stress failure and lung edema(22). Also, our preliminary findings indicated that endothelial Piezo1 might facilitate GVB disruption in response to elevated vascular pressures related to PH.

Here, we addressed the possibility that Piezo1, as a mechanical sensor of high vascular pressure in the PH condition, is responsible for GVB breakdown in cirrhosis. In further, we explored the key role and

underlying mechanism of Piezo1-mediated bi-directional GVB hyper-permeability in the intestinal and systemic inflammation that maybe the basis for the progress of liver cirrhosis. The study may provide new insights and potential targets for preventing the deterioration of liver cirrhosis with PH.

MATERIALS AND METHODS

Animals

C57BL/6 mice were supplied by Shulaibao Biotech Co., Ltd (Wuhan, China). Piezo1$^{flox/flox}$ mice (Cat. NO: NM-CKO-200275) were customized by Shanghai Model Organisms Center, Inc. (Shanghai, China). Cdh5-CreERT2 mice (Strain NO: T014691) were purchased from GemPharmatech Co., Ltd. (Nanjing, China). Piezo1$^{flox/flox}$ mice were crossed with Cdh5-CreERT2 mice to generate ECs-specific Piezo1-deficient mice (Piezo1$^{\triangle EC}$) with the deletion of exon 4 and 5 of Piezo1 cDNA (NCBI ID: 234839). The Piezo1$^{\triangle EC}$ mice were intraperitoneally given 1 mg of tamoxifen (dissolved in corn oil; Sigma-Aldrich Chemistry) for 5 days to induce the complete deletion of Piezo1 specific on ECs. The Piezo1$^{flox/flox}$ mice were used as controls (Piezo1^{WT}). The mice were raised in the SPF environment (Animal Experimental Center, Tongji Medical College, HUST, China) with a constant temperature and humidity, and with the light / dark alternate time 12h/12h. All animal experiments were approved by the Institutional Animal Care and Use Committee of Tongji Medical College, HUST, China.

CCl-induced Liver Cirrhosis Model

Liver cirrhosis model was established through the administration of carbon tetrachloride (CCl_4) in mice(31). CCl_4 (C822982, Macklin, China) was diluted at 5:5 (v/v) in olive oil (O815211, Macklin, China) for modeling. Male mice (8 weeks old) were injected subcutaneously with CCl_4 diluent at a dose of 3 ml/kg twice a week for 12 weeks. As a control, other mice administrated with 3 ml/kg olive oil only twice a week for 12 weeks. To further increase portal pressure, part of the CCl_4 mice were subjected partial portal vein ligation (26G) at the 8th week, while others conducted a sham operation as control.

Partial Portal Vein Ligation (PPVL)-induced PH Model

Mice model of pre-hepatic portal hypertension was induced by PPVL as previously described(32, 33). Briefly, mice were performed median laparotomy under anaesthesia, and the portal vein was carefully isolated. A blunt-tipped needle (26G or 27G) was placed on the portal vein, and a constricting ligature was conducted both on the needle and the portal vein with 7 – 0 silk. The needle was removed later on, leaving a calibrated stenosis (diameter about 0.46mm or 0.41mm) of the portal vein, and then the abdominal incision was sutured. A sham operation was performed in the control mice with portal vein isolated but not ligated. After a two-week recovery period following surgery, the mice were used for subsequent experimental testing.

Portal Venous Pressure Measurement

The portal pressure was measured via the water column method(32). The mice were anesthetized with pentobarbital sodium, performed laparotomy incision and the portal vein was dissociated. An 26G infusion cannula was cannulated into the portal vein, and connected to a glass-tube manometer with water column (containing heparin sodium physiological saline). The portal pressure was recorded as the height of water column when the water column in the glass-tube manometer was stayed stationary.

Assessment of Gut-Vascular Barrier Function

The function of GVB was assessed by detecting the endothelial PV1 expression, and measuring the macromolecular permeability from the gut to blood and from blood to the gut.

Endothelial PV1 expression. The PV1 distribution density was assessed via immunofluorescence, and present as the ratio of $PV1^+/CD31^+$ area in the ileal and colonic slices.

Permeability from the gut to blood. To assess the in-flux permeability of GVB, FITC-labeled dextran 70kDa (FD70, 2mg prepared in 2 ml physiological saline; Sigma-Aldrich Chemistry) was injected into a 4 cm-length intestinal loop (ligated at both ends with suture) through laparotomy incision under anesthesia(34). One hour later, the blood samples were collected from the abdominal aorta, and the plasma FD70 level was detected via a fluorescence microplate reader (BioTek Instruments, USA). Meanwhile, the liver and spleen tissues were obtained under light-proof conditions, and fixed with 4% paraformaldehyde, made into 20 μm frozen sections, then imaged on a confocal fluorescence microscopy (Olympus Corporation, Japan). The density of FD70 particles in the liver and spleen were quantified via ImageJ software (National Institutes of Health, USA).

Permeability from blood to the gut. To assess the out-flux permeability of GVB, Evans blue or FD70 was intravenous injected and the vascular leakage of these macromolecular was detected(34–36). (1) Evans blue (30 mg/kg in 100μl normal saline; Sigma-Aldrich Chemistry) was injected into the tail vein of mice. The mice were killed 20 min later, the ileal and colonic tissues (the same segment for each mouse) were removed, and then cut along the sagittal direction, removed the faeces and blotted dry. Tissues were immersed in 1ml formamide overnight at 55°C to extract the Evans blue dye in the ileum and colon. The content of Evans blue was measured via spectrophotometry at 600nm, and the result expressed as μg/mg tissue. (2) 200 μl FD70 (2 mg/ml in normal saline; Sigma-Aldrich Chemistry) was injected into the tail vein of mice. After 2 h post injection, the mice were anesthetized and performed cardiac perfusion with physiological saline. The ileal and colonic tissues (the same segment for each mouse) were removed, and then fixed in 4% paraformaldehyde for 24 h, made into 20 μm frozen sections. The vascular ECs were labeled by immunofluorescent with anti-CD31 primary antibody and Alexa Fluor 594-conjugated secondary antibody. The sections were imaged on a confocal laser scanning microscope (Nikon, Japan), and the FD70 fluorescent extravasation was observed. The FITC positive area represented the vascular leakage of FD70 was quantified using ImageJ software.

Assessment of Intestinal Epithelial Permeability

The function of intestinal epithelial barrier was assessed via detecting the plasma endotoxin (LPS) on portal vein, and measuring the trans-epithelial cell resistance (TER) and the permeability to macromolecules in an Ussing Chamber method.

Plasma endotoxin assay. Portal vein plasma were collected in endotoxin-free tubes and stored at − 80°C until assessment. LPS concentration was detected using a Mouse Endotoxin ELISA Kit (Bioswamp, China) following the manufacturer's instructions. In brief, 100 μl plasma sample was firstly reacted 100 μl limulus amebocyte lysate at 37°C for 5 min, incubated with 100 μl chromogenic substrate solution at 37°C for 5 min, and then terminated by reconstituted stop solution. The optical density (OD) was measured at 405 nm using a microplate reader (BIOBASE, China). Plasma endotoxin level was quantified against a standard curve.

Ussing chamber analysis. The intestinal mucosal patches were prepared by stripping the seromuscular layer as previously described(37). The intact mucosal patches were mounted on the sliders with a rectangular hole (opening area 0.15 cm^2) in the center, and the sliders were fixed on the U-type chambers filled with 37 ℃ oxygenated Krebs' solution at both the serosal and mucosal sides. Then, the U-type chambers were installed on an Ussing Chamber System (World Precision Instruments, USA). After a 20-min stability, the TER was recorded through the automatic voltage clamp model. To evaluate the mucosal-to-serosal flux of macromolecules, FITC-labeled dextran 4kDa (FD4, 1 mg/ml; Sigma-Aldrich Chemistry) was added into the mucosal side of the U-type chambers, and sampled from the serosal side every 30 min for a 2-h period. The FD4 concentration was further detected on a fluorescence microplate reader (BioTek Instruments, USA). The epithelial permeability was determined as the increase of FD4 intensity in the serosal side within 2 hours.

Cell Culture of Intestinal Microvascular ECs

ECs monolayer culture and interventions. Human intestinal microvascular endothelial cell (HIMECs; PriCells, China) were cultured in primary endothelial cell complete medium (MED-0002, PriCells) with growth supplement (SUP-0002, PriCells) of 5 ng/ml rh-VEGF, 5 ng/ml rh-EGF, 5 ng/ml rh-FGF, 15 ng/ml rh-IGF-1, 10 mM L-glutamine, 0.75 U/ml heparin sulfate, 1 μg/ml hydrocortisone and 50 μg/ml ascorbic acid at 37 ℃ in 5% CO_2. As reached 80% confluence, the cells were rinsed twice with PBS, digested with 0.125% trypsin for 2 min, and passaged at a 1:2 dilution ratio, and cultured for no more than 3 generations. ECs were seeded on transwell membrane or coverslips in 24-well plates as the requirement of different experiments. Upon formation of stable intercellular connections, the cells were subjected interventions of Yoda1 (1 μM, 5μM) or hydrostatic pressure (2cm, 15cm, 30cmH_2O) for 24 h for further detection, and preconditioned with siRNA transfection to silence Piezo1 or Vegfr2 when needed. Specially, the hydrostatic pressure was produced via an experimental apparatus (Fig. 6A) as previously described (38, 39). The culture chamber (a closed culture bottle) was filled with medium, where the cell-

planted transwell membrane or coverslip was placed. The height of the medium reservoir was adjusted to maintain the pressure in the culture (2cm, 15cm, 30cm). The medium in the culture chamber and the medium reservoir was circulated by a peristaltic pump to ensure gas exchange and maintain stable oxygen tension. The entire device was placed in the incubator with 37 ℃ and 5% CO_2.

Transmembrane resistance and permeability assay. ECs were inoculated on the transwell membrane with 0.4μm pore size (Corning, USA) to form an endothelial monolayer. The transendothelial electrical resistance (TEER) was measured using an EVOM2 volt-ohmmeter (World Precision Instruments, USA), and calculated as $\Omega \cdot cm^2$(40). A transwell with only culture medium was set as a blank control to measure the baseline membrane resistance. The TEER reached 180 $\Omega \cdot cm^2$ indicated formation of functional monolayer barrier, and then it could be used for further barrier studies. The transendothelial permeability was evaluated by apical-to-basolateral transmission of FITC-labeled bovine serum albumin (FITC-BSA; Solarbio Life Science). Briefly,10 mg/ml FITC-BSA was added into the upper compartment of the transwell chamber for 2 h, and then 100 μl medium was sampled at the lower compartment and detected FITC-BSA concentration via a Fluorescence Microplate Reader (BioTek Instruments, USA). The BSA throughput was calculated as the ratio between the fluorescence intensity in the lower chamber and upper chamber, and the data were presented as a percentage of the control(41, 42).

Small Interfering RNA (siRNA) Transfection

The gene silence of Piezo1 or Vegfr2 in ECs was achieved via specific siRNA. The siRNAs against human Piezo1, Vegfr2, and negative control were designed and chemically synthesized (Tsingke Biotech, China). The designed siRNAs were as follows: Piezo1-targeting siRNA (Piezo1-si) sequences were sense (5'-3') CUCAAGUACUUCAUCAACU(dT)(dT), antisense (5'-3') AGUUGAUGAAGUACUUGAG(dT)(dT), Gene ID: 9780; and Vegfr2-targeting siRNA (Vegfr2-si) sequences were sense (5'-3') GGAAAUCUCUUGCAAGCUA(dT)(dT), antisense (5'-3') UAGCUUGCAAGAGAUUUCC(dT)(dT), Gene ID: 3791. For cell transfection, ECs were seeded on BioFlex 6-well culture plates coated with type IV collagen. The cells were serum-starved for 6 hours, and transfected with 40 nM siRNA (Piezo1-si, Vegfr2-si, or control siRNA) via Lipofectamine™ 3000 reagent (L3000075, Invitrogen, Life Science) following the manufacturer's instructions. The mRNA and protein expression was detected by RT-qPCR and Western blot at 48 h post transfection to confirm effect of knockdown.

Data Availability

The supporting data for this study are available from the corresponding authors upon reasonable request. The expanded methods are provided in the Supplementary Methods.

Statistical Analysis

All data were presented as the mean ± SEM. Statistical analysis and graphic production were performed using GraphPad Prism 10 (GraphPad Software, USA). The Shapiro-Wilk test and Brown-Forsythe test

were employed to assess the normality of data distribution and the homogeneity of variances, respectively. Comparisons between groups were conducted performed using unpaired two-tailed Student's t-test (for two groups) or one-way analysis of variance (ANOVA) followed by least significant difference test (for multiple groups), if the data conformed to normal distribution and equal variance; otherwise, the non-parametric Mann-Whitney U test or Kruskal-Wallis test with Dunn's post hoc correction was applied accordingly. Pearson correlation was applied to assessed the correlations between parameters. A $P < 0.05$ was considered statistically significant.

RESULTS

Portal Hypertension Mediated GVB Disruption Promoted Intestinal and Systemic Inflammation in CCl_4-induced Liver Cirrhosis

Liver cirrhosis and related PH was induced by CCl4 administration (Fig. 1A). CCl_4 induced significant liver injury and fibrosis, with diffuse inflammatory cell infiltration and vacuolar fat changes (Fig. 1B), elevated serum ALT and AST levels (Fig. 1D), increased areas of collagen (Sirius red positive, Fig. 1E) and α-SMA expression (Fig. 1F). The portal venous pressure markedly increased in CCl_4 mice, and further elevated in the CCl_4 mice with PPVL (Fig. 1C). PH was associated with hepatic injury, manifesting as more severe inflammatory infiltration and elevation of serum ALT and AST in CCl_4+PPVL mice compared with CCl_4 mice (Fig. 1B, 1D).

There were obvious intestinal and systemic inflammation in CCl_4-induced liver cirrhosis, and aggravate in the CCl_4+PPVL mice. The levels of plasma endotoxin and circulating inflammatory cytokines, including TNF-α, IL-1β and IL-6, were increased in CCl_4 mice and CCl_4+PPVL mice (Fig. 1G, 1H), which were positive correlated with the portal venous pressure (Figure S2). Furthermore, the microvascular dilation, inflammatory infiltration and the concentrations of inflammatory TNF-α, IL-1β and IL-6 were also markedly increased in ileum and colon of CCl_4 mice and CCl_4+PPVL mice (Fig. 1I-J; Figure S3). And the intestinal inflammation was accompanied by disruption of mucosal epithelial barrier, with reduced TER and increased FD4 permeability (Fig. 1K-L). All above indicated that PH may contribute to the local inflammatory injury and leaky gut, and meanwhile promote the circulating inflammation, in status of liver cirrhosis.

Importantly, it observed significantly GVB disruption in CCl_4 mice, and more serious GVB damage in CCl_4+PPVL mice. As it shown, there was increased FD70 density detected in liver and spleen when administered through the intestine in CCl_4 mice (Fig. 1M, 1P-Q), which implied increased influx of enterogenous macromolecules into the bloodstream. The ileal and colonic PV1 expression, a marker of endothelial permeability, was also increased in CCl_4 mice which confirmed the GVB disruption in liver cirrhosis (Fig. 1N, 1R; Figure S4). On the other hand, the vascular leakage of circulating macromolecules

into the gut was also increased in CCl_4 mice, with raised FD70 (Fig. 1O, 1S) and evans blue (Fig. 1T) levels in the ileal and colonic mucosa when administered via tail-vein injection. Moreover, the GVB disruption was more remarkable in the CCl_4+PPVL mice relative to the sham group. It further verified the inward and outward hyper-permeability of GVB in portal hypertension and liver cirrhosis.

Impaired GVB Initiates Gut Inflammation and Leakage, and Led to Systemic Injury in PPVL-induced Portal Hypertension

Prehepatic PH was induced via partial portal vein ligation with 26G and 27G needles (Fig. 2A). PPVL led to significant increase in portal venous pressure (Fig. 2C), and presented with local inflammatory cell infiltration and blood stagnation in the hepatic sinusoid (Fig. 2B), but without elevation of serum ALT and AST levels (Fig. 2D). Similarly, PPVL-induced PH appeared increased levels of plasma LPS and pro-inflammatory TNF-α, IL-1β and IL-6 (Fig. 2E-F), as well as inflammatory infiltration and increased concentrations of TNF-α, IL-1β and IL-6 in ileum and colon (Fig. 2G-H; Figure S5) with reduced TER and increased FD4 permeability (Fig. 2I-J). The GVB dysfunction was also observed in PH mice induced by PPVL, including increased endothelial PV1 expression in the ileum and colon (Fig. 2L, 2P; Figure S6), increased FD70 permeability from the gut to blood (Fig. 2K, 2N-O), and increased FD70 and evans blue leakage from blood to the gut (Fig. 2M, 2Q-R). It again pointed out that PH destroyed the GVB may initiate the gut inflammation and leakage, and cause systemic inflammation and injury.

Upregulation of Piezo1 in the Intestinal Microvascular ECs Under Portal Hypertension of CCl_4 and PPVL Mice

Expression of mechanosensitive Piezo1 was up-regulated in the intestinal microvascular ECs at PH state. As it shown with immunofluorescence, Piezo1 intensity in $CD31^+$ ECs of the ileum and colon was enhanced in both the CCl_4 and PPVL induced PH mice (Fig. 3A). Additionally, we further identified the $CD45^-CD90^-CD31^+$ vascular ECs in the ileum and colon via flow cytometry (Figure S7; Figure S8). The results revealed an increased average expression of Piezo1 in the intestinal vascular ECs from the CCl_4 and PPVL mice compared with the sham controls (Fig. 3B-I). It indicated that Piezo1 may mediate the pressure sensation of intestinal vascular ECs in PH and liver cirrhosis.

Endothelial Piezo1 Knockout Improved GVB Dysfunction and Leaky Gut Induced by Portal Hypertension

Silence of endothelial Piezo1 effectively improved the GVB dysfunction, and relieved the intestinal and systemic inflammation in CCl_4 and PPVL induced PH mice. The PH-induced high expression of endothelial PV1 in the ileum and colon declined in the $Piezo1^{\Delta EC}$ mice compared to the $Piezo1^{WT}$ mice (Fig. 4L, 4O; Figure S11). In $Piezo1^{\Delta EC}$ mice, PH-induced GVB hyper-permeability was obviously suppressed, which presented as decreased FD70 permeability from the gut to blood (Fig. 4J, 4M-N), and reduced FD70 and evans blue leakage from blood to the gut (Fig. 4K, 4P-Q). Piezo1 knockout relived the

GVB function which was associated with declined circulating levels of LPS and pro-inflammatory cytokines TNF-α, IL-1β and IL-6 in CCl_4 and PPVL mice (Fig. 4D-E), and as well reduced hepatic inflammatory infiltration and injury (Fig. 4A-B; Figure S9). Moreover, the restored GVB function also improved the intestinal inflammation, reduced mucosal TNF-α, IL-1β and IL-6 secretion (Fig. 4H-I; Figure S10), and recovered epithelial barrier and lessened gut leakage in the CCl_4 and PPVL mice (Fig. 4F-G).

Piezo1 Activation by Yoda1 and Hydrostatic Pressure Triggered the Increased Permeability of Intestinal Microvascular ECs

Yoda1 activated Piezo1 channel and triggered Ca^{2+} influx in intestinal microvascular ECs (Fig. 5A-C). Piezo1 activation significantly increased the permeability of endothelial barrier, with decreased transendothelial cell resistance (TER) and increased passage of macromolecular FITC-BSA (Fig. 5D-E), and also with increased PV1 levels and down-regulated expression of junctional proteins such as VE-cadherin, occludin, claudin-1, ZO-1 and JAM-A (Fig. 5F-L).

Additionally, the hydrostatic pressure (2cm, 15cm, and 30cmH_2O) induced Piezo1 activation was further tested (Fig. 6A). It indicated that elevated pressure stimulated Piezo1 expression and Ca^{2+} influx in intestinal ECs, which could be obviously inhibited by Piezo1 silence with specific siRNA (Fig. 6B-D). Also, there was marked reduce in TER and increase in FITC-BSA permeability in ECs as the pressure stimulus elevated (Fig. 6E-F). High hydrostatic pressure promoted the expression of PV1, and disrupted the adhesion and tight junctions among ECs, with weak expression of VE-cadherin, occludin, claudin-1, ZO-1 and JAM-A (Fig. 6G-L; Figure S14). The pressure-mediated hyper-permeability and junctional damage of ECs could be blocked by Piezo1-siRNA.

Piezo1 Promoted Endothelial Hyperpermeability and GVB Dysfunction via Activating the VEGFR2 Signaling

The differential genes were identified and exhibited via volcano plot based on the RNA sequencing data (Fig. 7A), and the GSEA analysis illustrated the enrichment of the VEGF signaling pathway and the VEGFR regulation pathway in ECs treated with Yoda1 (Fig. 7B-C; Figure S15). The RT-PCR assay further confirmed that Yoda1 and hydrostatic pressure significantly promoted the mRNA expression in ECs, which could be blocked by Piezo1-siRNA (Fig. 7D, 7N). In addition, Piezo1 activation by Yoda1 (1μM and 5μM) and hydrostatic pressure (15cm and 30cmH_2O) facilitated the endothelial expression of VEGFR2 (Fig. 7E-H), particularly promoted the phosphorylated level of VEGFR2 (Fig. 7I-M). And hydrostatic pressure (30cmH_2O) induced high expression of VEGFR2 and p-VEGFR2 was obviously inhibited by Piezo1-siRNA. In vivo study also indicated a remarkable increase of VEGFR2 expression in ileal and colonic vascular ECs in CCl_4 and PPVL mice, while it was repressed in the Piezo1$^{\Delta EC}$ mice (Fig. 7O; Figure S16). The mRNA and protein expression of VEGFR2, and the phosphorylation level, in the gut of CCl_4 and PPVL mice were evidently inhibited in the Piezo1 knockout state (Fig. 7P-T; Figure S16). All

above suggested that endothelial Piezo1 may promote the GVB dysfunction via activating the VEGFR2 signaling.

Silence of VEGFR2 Alleviated Piezo1-mediated Dysfunction and Hyper-permeability of Intestinal Microvascular ECs

EC-model with silence of VEGFR2 was successfully established via specific siRNA (Fig. 8A-E; Figure S17). It demonstrated that VEGFR2 knockdown ameliorated the dysfunction of endothelial barrier induced by Yoda1 (5μM) and hydrostatic pressure (30cmH_2O), with increased TER and decreased FITC-BSA permeability (Fig. 8G-H). Moreover, VEGFR2-siRNA inhibited the PV1 expression in ECs upon Piezo1 activation by Yoda1 and hydrostatic pressure, and it in turn restored the cell junctions by promoting the expression of VE-cadherin, occludin, claudin-1, ZO-1 and JAM-A (Fig. 8F, 8I-N). These further clarified the role of VEGFR2 activation in Piezo1-induced hyper-permeability of intestinal microvascular ECs and GVB dysfunction.

DISCUSSION

Gut dysfunction played an important role in the progression of chronic liver disease and cirrhosis, due to the closely anatomical and functional relations of the gut-liver axis(8, 43). The degeneration of multiple intestinal barriers, including the biochemical, immunological and physical barrier, has been identified in liver injury(44, 45). It was highly concerned but several questions are still open, especially for the newly defined GVB which is last key guard from the intestine to liver. Here, we focused on the GVB disruption, to elucidate its role and mechanism in the development of liver cirrhosis.

GVB breakdown was remarkable in CCl_4-induced cirrhosis mice, presented as upregulated endothelial PV1 expression, and increased permeability to macromolecular particles such as LPS, FD70 and Evans blue. The hyper-permeability of GVB was responsible for the dissemination of luminal bacteria in experimental cirrhosis(10, 11). Normally, the invaded pathogens and antigens escaped from the epithelial barrier are denied entry to the internal environment by GVB, and are finally clear by the mucosal immune system(15, 46). This highlighted the importance of GVB integrity in preventing the aggravation of liver cirrhosis and systemic inflammatory damages.

As we shown, the GVB manifested as bi-directional hyper-permeability in CCl_4 mice, namely, increased passage from the gut to blood (inward) and also increased leakage from blood to the gut (outward). On the one aspect, the increased in-flux permeability of GVB directly resulted in bacterial translocation to the portal vein, which may further give rise to liver injury with increased ALT and AST levels, increased hepatic inflammation and fibrosis, and also systemic inflammation with increased levels of serum IL-1β, IL-6 and TNF-α. On the other hand, the raised out-flux permeability of GVB with microvascular leakage may initiate local inflammation in the intestine and trigger or aggravate epithelial leakage. It was true

that GVB damage was associated with increased inflammatory infiltration, and then decreased TER and elevated epithelial permeability to FD4 in ileum and colon. This may also be one potential explanation for the cause of intestinal damage and leaky gut in liver cirrhosis. The epithelial leakage, in turn, leads to more entries of luminal antigens forming a vicious cycle of systemic damage.

Portal hypertension was associated with GVB disruption in cirrhosis. Compared with the CCl_4 mice, the GVB damage was more evident in CCl_4+PPVL mice, with more obvious intestinal and systemic inflammation and injury. Also, the extent of GVB damage was positive correlated with portal pressure in PPVL-induced prehepatic PH mice. As increasing portal pressure, the intestinal and systemic inflammation deteriorated in PH status, with raised plasma endotoxin and levels of local and serum cytokines such as IL-1β, IL-6 and TNF-α. These findings indicated the role of pressure-mediated GVB disruption in liver cirrhosis with PH. Similarly, it was reported that elevated microvessel pressure induced lung endothelial hyper-permeability and edema formation via disruption of adherens junction(22, 23). Intraluminal pressure remodeled the endothelial tissue, and regulated their barrier function via thinned junctions(47). Our in vitro studies further revealed that elevated hydrostatic pressure destroyed the barrier function of intestinal microvascular ECs monolayer, with increased permeability to FITC-BSA and declined transendothelial resistance. Hydrostatic pressure facilitated endothelial barrier damage by increasing the expression of PV1, and breaking the endothelial adherens and tight junctions. Combined, PH-induced breakdown of endothelial integrity and increase of GVB permeability could be a potential explanation for the progress of liver cirrhosis and related systemic injury.

The mechanism of endothelial sense to PH and subsequent GVB collapse was largely unknown. Notably, the mechanosensitive Piezo1 channel is distributed in ECs that directly sensing the mechanical stimuli, such as hydrostatic pressure, shear stress and substrate stiffness(48, 49). Piezo1 is crucial for the homeostasis and angiogenesis of various vascular endothelium(22, 24, 27), including the intestinal microvessel ECs(28). Endothelial Piezo1 stimulated angiogenesis to offer protection against intestinal ischemia-reperfusion injury(28). Piezo1-mediated mechanotransduction contributes to endothelial inflammation activated by disturbed blood flow(30, 50). Deletion of endothelial Piezo1 effectively prevented pressure-induced vascular hyper-permeability and lung edema(22). The expression of Piezo1 on intestinal vessel ECs was upregulated in CCl_4- and PPVL-induced PH mice. And, specific knockout of Piezo1 in ECs improved the GVB function in PH mice, meanwhile inhibited the systemic and intestinal inflammation, and relieved the epithelial barrier injury. This further indicated the potential role of Piezo1 in PH-induced GVB impairment and related mucosal and circulating inflammation. It was further verified that Piezo1 activation by Yoda1 or hydrostatic pressure destroyed the barrier function of intestinal microvascular ECs monolayer, which could be alleviated by Piezo1 silence with specific siRNA. Also, activation of Piezo1 by ultrasonic stimulation promoted the hyper-permeability in human umbilical vein ECs (HUVECs), while the suppression of Piezo1 showed a decline in cell permeability(51). Collectively, Piezo1 acted as a key sensor to PH and mediated the GVB impairment in liver cirrhosis, which could be a promising pharmacologic target to modulated GVB integrity.

Piezo1 activation in ECs by Yoda1 upregulated the VEGF and downstream signaling pathway and increased the expression of VEGFR2, deriving from the transcriptome results. Endothelial Piezo1 triggered VEGF/myc signaling by enhancing Ca^{2+} influx could be responsible for driving the angiogenesis(52). Piezo1 promoted angiogenesis in ileal ECs through the activation of the Ca^{2+}/HIF-1α/VEGF pathway during intestinal ischemia-reperfusion injury(28). These data indicated the compact link of Piezo1 and VEGF signaling in endothelial function. We further confirmed that activation of Piezo1 by Yoda1 or hydrostatic pressure stimulated Ca^{2+} influx, and promoted the expression and phosphorylation of VEGFR2 in ECs, which could be repressed by Piezo1-siRNA. Moreover, the high expression and activation of VEGFR2 in the ileum and colon of CCl_4 and PPVL mice were also inhibited in Piezo1$^{\Delta EC}$ mice. It also prompted that Piezo1/VEGFR2 collaboration may be involved in regulating the barrier function of ECs.

The VEGFR2 kinase signaling is an important regulator of vascular permeability, however, the effect varies in different situations. For example, disrupt blood-retinal barrier function of diabetic retinopathy(53), promote vascular leakage and edema in myocardial infarction(54), strengthen retinal endothelial barrier via endothelial-pericyte interaction(55), and restore pulmonary microvascular barrier following ischemia reperfusion injury(56). Excessive VEGFR2 trafficking to the cell surface mediated vascular permeability, while inhibited this VEGFR2 recycling mitigated vascular leakage associated with inflammatory diseases(57). In intestinal microvascular ECs, as we shown, inhibition of VEGFR2 with siRNA knockdown protected Yoda1 and hydrostatic pressure induced barrier disruption, through inhibiting the expression of PV1, enhancing the adherens junctions (VE-cadherin) and tight junctions (occludin, claudin-1, ZO-1 and JAM-A). Piezo1 is required in force-induced Ca^{2+}-dependent remodelling of cell-cell junctions and associated cytoskeleton, especially for adherens junctions(58). Piezo1 sensing of high vascular pressures at the endothelial surface may promote disassembly of adherens junctions(22, 59). These further clarified the role of VEGFR2 activation in Piezo1-induced hyper-permeability of intestinal microvascular ECs and GVB dysfunction.

This study provided a preliminary image that endothelial Piezo1 mediated GVB dysfunction in PH and promoted deterioration of liver cirrhosis. Nevertheless, several limitations should be acknowledged, which also offered the possible directions for future research. Firstly, our study focused on the role of Piezo1 in ECs, but did not preclude the involvement of other mechanosensitive channels or receptors(60) that may be responsible for pressure-induced endothelial hyperpermeability. Even so, the molecular pathway of Piezo1 in GVB impairment was currently limited, which should be multifaceted and requires further research to elucidate. Secondly, the actions of Piezo1 in modulating GVB function should be validated in PH patients with liver cirrhosis and related clinical manifestations of intestinal and systematic damage, for instance, through the study of gastrointestinal biopsy under endoscopy or surgery. And finally, the specific monoclonal antibody or fusion protein against Piezo1 is urgently needed, especially for the intestinal ECs-specific blocker with good in vivo safety and efficacy.

In summary, we expounded that Piezo1 contributed to PH-induced damage of intestinal microvascular ECs and GVB dysfunction in cirrhosis via recruiting and activating the VEGFR2 signaling. Especially, the outward (from blood to the gut) and inward (from the gut to blood) hyper-permeability of GVB in PH status may initiate the intestinal inflammation, trigger or aggravate epithelial leakage, and in turn lead to more convenient bacterial translocation into the portal vein, facilitate liver and systemic damage, forming a vicious cycle. So that, Piezo1 mediated bi-directional hyper-permeability of the GVB should be a novel explanation and potential therapeutic target for preventing the exacerbation of liver cirrhosis with PH.

Abbreviations

CCl_4, carbon tetrachloride;

PPVL, partial portal vein ligation;

PH, portal hypertension;

ALT, alanine aminotransferase;

AST, aspartate aminotransferase;

GVB, gut-vascular barrier;

ECs, endothelial cells;

HIMECs, human intestinal microvascular endothelial cells;

LPS, lipopolysaccharide;

FD4, fluorescein isothiocyanate-labeled dextran 4kDa;

FD70, fluorescein isothiocyanate-labeled dextran 70kDa;

BSA, bovine serum albumin;

TER, trans-epithelial/endothelial cell resistance;

PV1, plasmalemma vesicle-associated protein 1;

VEGFR2, vascular endothelial growth factor receptor 2.

DEGs, differential expression genes.

Declarations

Acknowledgements

We thank Dr. Liuying Chen (Division of Gastroenterology, Union Hospital, Tongji Medical College, Huazhong University of Science and Technology) for providing HIMECs and technical assistances.

Author Contributions

Xiao Z: methodology, investigation, validation, data curation, writing - original draft; **He J:** software, formal analysis; **Tian W:** investigation; **Du L:** investigation; **Wang R:** validation; **Bai T:** software, formal analysis; **Qian W:** methodology, resources; **Song J:** conceptualization, supervision, writing - review & editing; **Hou X:** project administration,funding acquisition, writing - review & editing; **Zhang L:** funding acquisition, conceptualization, methodology, investigation, data curation, writing - original draft.

Ethical Statement

This study was approved by the Animal Care and Use Committee, Tongji Medical College, Huazhong University of Science and Technology, China (Approval NO:3372).

Conflicts of Interest Statement

The authors declare that they had full control over the data and complete access to the data, and no competing interest declared.

Transcript profiling

The raw RNA-seq data was published in the Sequence Read Archive (SRA) database with Bioproject number PRJNA1415200.

Data Availability Statement

The original contributions presented in this study are included in this article and supplementary material, further inquiries can be directed to the corresponding authors.

Grant support

This study was funded by grants from the National Natural Science Foundation of China (NSFC), China (No: 82470566, 81800463).

References

1. Villanueva C, Tripathi D, Bosch J. Preventing the progression of cirrhosis to decompensation and death. Nat Rev Gastroenterol Hepatol 2025;22:265–280.
2. Tapper EB, Parikh ND. Diagnosis and Management of Cirrhosis and Its Complications: A Review. JAMA 2023;329:1589–1602.

3. Poordad FF. Presentation and complications associated with cirrhosis of the liver. Curr Med Res Opin 2015;31:925–937.
4. Trebicka J, Bork P, Krag A, Arumugam M. Utilizing the gut microbiome in decompensated cirrhosis and acute-on-chronic liver failure. Nat Rev Gastroenterol Hepatol 2021;18:167–180.
5. Trebicka J, Hernaez R, Shawcross DL, Gerbes AL. Recent advances in the prevention and treatment of decompensated cirrhosis and acute-on-chronic liver failure (ACLF) and the role of biomarkers. Gut 2024;73:1015–1024.
6. Trebicka J, Macnaughtan J, Schnabl B, Shawcross DL, Bajaj JS. The microbiota in cirrhosis and its role in hepatic decompensation. J Hepatol 2021;75 Suppl 1:S67-S81.
7. Bhargava S, Rao Z, Vanholder R, Tacke F, Noels H, Jankowski V, Hermann J, et al. The impact of gut-liver-derived mediators on the organ crosstalk with brain, heart, and kidney: A systematic review. Mol Metab 2025;103:102295.
8. Chen Z, Liao S, Wu S, Chen S, Tang Q, Zhou L, Li X, et al. The Gut–Liver Axis in Liver Disease: Molecular Mechanisms and Therapeutic Targets. MedComm (2020) 2025;6:e70458.
9. Albillos A, de Gottardi A, Rescigno M. The gut-liver axis in liver disease: Pathophysiological basis for therapy. J Hepatol 2020;72:558–577.
10. Sorribas M, Jakob MO, Yilmaz B, Li H, Stutz D, Noser Y, de Gottardi A, et al. FXR modulates the gut-vascular barrier by regulating the entry sites for bacterial translocation in experimental cirrhosis. J Hepatol 2019;71:1126–1140.
11. Smets L, Viola MF, Boesch M, Raman J, Van Melkebeke L, Nobis M, Flint E, et al. Intestinal blood vessel-associated macrophages and gut-vascular barrier dysfunction in cirrhosis. Gut 2025.
12. Spadoni I, Zagato E, Bertocchi A, Paolinelli R, Hot E, Di Sabatino A, Caprioli F, et al. A gut-vascular barrier controls the systemic dissemination of bacteria. Science 2015;350:830–834.
13. Liu S, Song P, Sun F, Ai S, Hu Q, Guan W, Wang M. The concept revolution of gut barrier: from epithelium to endothelium. Int Rev Immunol 2021;40:401–408.
14. Ungaro F, Tacconi C, D'Alessio S. Beyond Intestinal Barrier: The Blood Endothelium as a Second Wall of Defense Against Bacterial Invasion. Gastroenterology 2016;150:1678–1680.
15. Cheng C, Tan J, Qian W, Zhang L, Hou X. Gut inflammation exacerbates hepatic injury in the high-fat diet induced NAFLD mouse: Attention to the gut-vascular barrier dysfunction. Life Sci 2018;209:157–166.
16. Mouries J, Brescia P, Silvestri A, Spadoni I, Sorribas M, Wiest R, Mileti E, et al. Microbiota-driven gut vascular barrier disruption is a prerequisite for non-alcoholic steatohepatitis development. J Hepatol 2019;71:1216–1228.
17. Di Tommaso N, Santopaolo F, Gasbarrini A, Ponziani FR. The Gut-Vascular Barrier as a New Protagonist in Intestinal and Extraintestinal Diseases. Int J Mol Sci 2023;24.
18. Zhu F, Zheng S, Zhao M, Shi F, Zheng L, Wang H. The regulatory role of bile acid microbiota in the progression of liver cirrhosis. Front Pharmacol 2023;14:1214685.

19. Xie K, Zhang Y, Tan S, Luo J, Ou X, Tan S. Gut microbiota involvement in the alteration of inflammatory cell infiltration and gut barrier integrity in liver cirrhosis. Biomed Rep 2025;23:193.
20. De Palma GD, Rega M, Masone S, Persico F, Siciliano S, Patrone F, Matantuono L, et al. Mucosal abnormalities of the small bowel in patients with cirrhosis and portal hypertension: a capsule endoscopy study. Gastrointest Endosc 2005;62:529–534.
21. Xiao B. Mechanisms of mechanotransduction and physiological roles of PIEZO channels. Nat Rev Mol Cell Biol 2024;25:886–903.
22. Friedrich EE, Hong Z, Xiong S, Zhong M, Di A, Rehman J, Komarova YA, et al. Endothelial cell Piezo1 mediates pressure-induced lung vascular hyperpermeability via disruption of adherens junctions. Proc Natl Acad Sci U S A 2019;116:12980–12985.
23. Chen J, Miao J, Zhou D, Liao J, Wang Z, Lin Z, Zhang C, et al. Upregulation of mechanosensitive channel Piezo1 involved in high shear stress-induced pulmonary hypertension. Thromb Res 2022;218:52–63.
24. Li X, Wang M, Seehaber J, Stuhldreier C, Butt YA, Pacia MZ, Hollmann MW, et al. Sodium glucose co-transporter 2 inhibitor empagliflozin prevents endothelial dysfunction induced by oscillatory shear stress. Biomed Pharmacother 2025;192:118670.
25. Harraz OF, Hashad AM. Brain Capillary Ion Channels: Physiology and Channelopathies. Physiology (Bethesda) 2026;41:0.
26. Lim XR, Abd-Alhaseeb MM, Ippolito M, Koide M, Senatore AJ, Plante C, Hariharan A, et al. Endothelial Piezo1 channel mediates mechano-feedback control of brain blood flow. Nat Commun 2024;15:8686.
27. Fu H, Yu Y, Wang S, Xu P, Sun Y, Li J, Ge X, et al. Piezo1 disrupts blood-brain barrier via CaMKII/Nrf2 in ischemic stroke. Cell Mol Life Sci 2025;82:259.
28. Wang C, Luo S, Yan Y, Li J, Niu W, Hong T, Hao K, et al. Endothelial Piezo1 stimulates angiogenesis to offer protection against intestinal ischemia-reperfusion injury in mice. Mol Med 2025;31:147.
29. Albarran-Juarez J, Iring A, Wang S, Joseph S, Grimm M, Strilic B, Wettschureck N, et al. Piezo1 and G(q)/G(11) promote endothelial inflammation depending on flow pattern and integrin activation. J Exp Med 2018;215:2655–2672.
30. Lan Y, Lu J, Zhang S, Jie C, Chen C, Xiao C, Qin C, et al. Piezo1-Mediated Mechanotransduction Contributes to Disturbed Flow-Induced Atherosclerotic Endothelial Inflammation. J Am Heart Assoc 2024;13:e035558.
31. Xu T, Lu Z, Xiao Z, Liu F, Chen Y, Wang Z, Zhu S, et al. Myofibroblast induces hepatocyte-to-ductal metaplasia via laminin-avbeta6 integrin in liver fibrosis. Cell Death Dis 2020;11:199.
32. Hassan M, Moghadamrad S, Sorribas M, Muntet SG, Kellmann P, Trentesaux C, Fraudeau M, et al. Paneth cells promote angiogenesis and regulate portal hypertension in response to microbial signals. J Hepatol 2020;73:628–639.
33. Schwabl P, Hambruch E, Seeland BA, Hayden H, Wagner M, Garnys L, Strobel B, et al. The FXR agonist PX20606 ameliorates portal hypertension by targeting vascular remodelling and sinusoidal

dysfunction. J Hepatol 2017;66:724–733.

34. Chen Y, Zhang L, Hong G, Huang C, Qian W, Bai T, Song J, et al. Probiotic mixtures with aerobic constituent promoted the recovery of multi-barriers in DSS-induced chronic colitis. Life Sci 2020;240:117089.
35. Huang J, Kelly CP, Bakirtzi K, Villafuerte Galvez JA, Lyras D, Mileto SJ, Larcombe S, et al. Clostridium difficile toxins induce VEGF-A and vascular permeability to promote disease pathogenesis. Nat Microbiol 2019;4:269–279.
36. Liu C, Xiao Z, Du L, Zhu S, Xiang H, Wang Z, Liu F, et al. Interferon-gamma secreted by recruited Th1 cells in peritoneal cavity inhibits the formation of malignant ascites. Cell Death Discov 2023;9:25.
37. Li Y, Jiang Y, Zhang L, Qian W, Hou X, Lin R. Exogenous l-fucose protects the intestinal mucosal barrier depending on upregulation of FUT2-mediated fucosylation of intestinal epithelial cells. FASEB J 2021;35:e21699.
38. Lei Y, Rajabi S, Pedrigi RM, Overby DR, Read AT, Ethier CR. In vitro models for glaucoma research: effects of hydrostatic pressure. Invest Ophthalmol Vis Sci 2011;52:6329–6339.
39. Ishikawa M, Yoshitomi T, Zorumski CF, Izumi Y. Experimentally Induced Mammalian Models of Glaucoma. Biomed Res Int 2015;2015:281214.
40. Ren X, Shi B, Chang Z, Zhang J, Wang S, Liu R, Sang M, et al. Relationship between pathogenic E.coli O78-induced intestinal epithelial barrier damage and Zonulin expression levels in yaks. Front Cell Infect Microbiol 2024;14:1456356.
41. Yang D, Liu J, Tian C, Zeng Y, Zheng YH, Fang Q, Li HH. Epigallocatechin gallate inhibits angiotensin II-induced endothelial barrier dysfunction via inhibition of the p38 MAPK/HSP27 pathway. Acta Pharmacol Sin 2010;31:1401–1406.
42. Yang D, Xie P, Guo S, Li H. Induction of MAPK phosphatase-1 by hypothermia inhibits TNF-alpha-induced endothelial barrier dysfunction and apoptosis. Cardiovasc Res 2010;85:520–529.
43. Xing Y, Ou Y, Wang Y, Hou L, Zhu J. New insights into gut-liver axis in advanced liver diseases: A promising therapeutic target. Biochem Pharmacol 2025;242:117284.
44. Liu L, Yin M, Gao J, Yu C, Lin J, Wu A, Zhu J, et al. Intestinal Barrier Function in the Pathogenesis of Nonalcoholic Fatty Liver Disease. J Clin Transl Hepatol 2023;11:452–458.
45. Chopyk DM, Grakoui A. Contribution of the Intestinal Microbiome and Gut Barrier to Hepatic Disorders. Gastroenterology 2020;159:849–863.
46. Mihailuta F, Chioasca TP, Onofrei Popa A, Chelmu Voda C, Balta AAS, Arghir OC, Voinescu DC. The Vulnerable Vascular Network: Endothelial Dysfunction as a Central Driver of Intestinal Inflammation-A Systematic Review. Biomedicines 2025;13.
47. Cacheux J, Bancaud A, Alcaide D, Suehiro JI, Akimoto Y, Sakurai H, Matsunaga YT. Endothelial tissue remodeling induced by intraluminal pressure enhances paracellular solute transport. iScience 2023;26:107141.

48. Mandrycky CJ, Ishida T, Merkel T, Rayner SG, Heck AM, Hadland B, Zheng Y. Under pressure: integrated endothelial cell response to hydrostatic and shear stresses. Vasc Biol 2025;7.
49. Lai A, Zhou Y, Thurgood P, Chheang C, Chandra Sekar N, Nguyen N, Peter K, et al. Endothelial Response to the Combined Biomechanics of Vessel Stiffness and Shear Stress Is Regulated via Piezo1. ACS Appl Mater Interfaces 2023;15:59103–59116.
50. Wang S, Chennupati R, Kaur H, Iring A, Wettschureck N, Offermanns S. Endothelial cation channel PIEZO1 controls blood pressure by mediating flow-induced ATP release. J Clin Invest 2016;126:4527–4536.
51. Zhang L, Liu X, Gao L, Ji Y, Wang L, Zhang C, Dai L, et al. Activation of Piezo1 by ultrasonic stimulation and its effect on the permeability of human umbilical vein endothelial cells. Biomed Pharmacother 2020;131:110796.
52. Lv W, Yang F, Ge Z, Xin L, Zhang L, Zhai Y, Liu X, et al. Aberrant overexpression of myosin 1b in glioblastoma promotes angiogenesis via VEGF-myc-myosin 1b-Piezo1 axis. J Biol Chem 2024;300:107807.
53. Liu S, Hou J, Tao Y, Xu Y, Liu J, Lin S, Tao L, et al. ELF3-regulated PES1 targets VEGFR2 to mediate angiogenesis and retinal inner barrier injury in diabetic retinopathy. J Transl Med 2025;23:1309.
54. Li X, Redfors B, Sainz-Jaspeado M, Shi S, Martinsson P, Padhan N, Scharin Tang M, et al. Suppressed Vascular Leakage and Myocardial Edema Improve Outcome From Myocardial Infarction. Front Physiol 2020;11:763.
55. Lin YY, Warren E, Macklin BL, Ramirez L, Gerecht S. Endothelial-Pericyte Interactions Regulate Angiogenesis Via VEGFR2 Signaling During Retinal Development and Disease. Invest Ophthalmol Vis Sci 2025;66:45.
56. Walsh D, Kostyunina DS, Blake A, Boylan J, McLoughlin P. Shear stress-induced restoration of pulmonary microvascular endothelial barrier function following ischemia reperfusion injury requires VEGFR2 signaling. Am J Physiol Lung Cell Mol Physiol 2025;328:L389-L404.
57. Cho HD, Nhan NTT, Zhou C, Tu K, Nguyen T, Sarich NA, Yamada KH. KIF13B mediates VEGFR2 recycling to modulate vascular permeability. Cell Mol Life Sci 2023;80:91.
58. Chuntharpursat-Bon E, Povstyan OV, Ludlow MJ, Carrier DJ, Debant M, Shi J, Gaunt HJ, et al. PIEZO1 and PECAM1 interact at cell-cell junctions and partner in endothelial force sensing. Commun Biol 2023;6:358.
59. Jiang L, Zhang Y, Lu D, Huang T, Yan K, Yang W, Gao J. Mechanosensitive Piezo1 channel activation promotes ventilator-induced lung injury via disruption of endothelial junctions in ARDS rats. Biochem Biophys Res Commun 2021;556:79–86.
60. Yang H, Hou C, Xiao W, Qiu Y. The role of mechanosensitive ion channels in the gastrointestinal tract. Front Physiol 2022;13:904203.
61. FIFURE LEGENDS

Figures

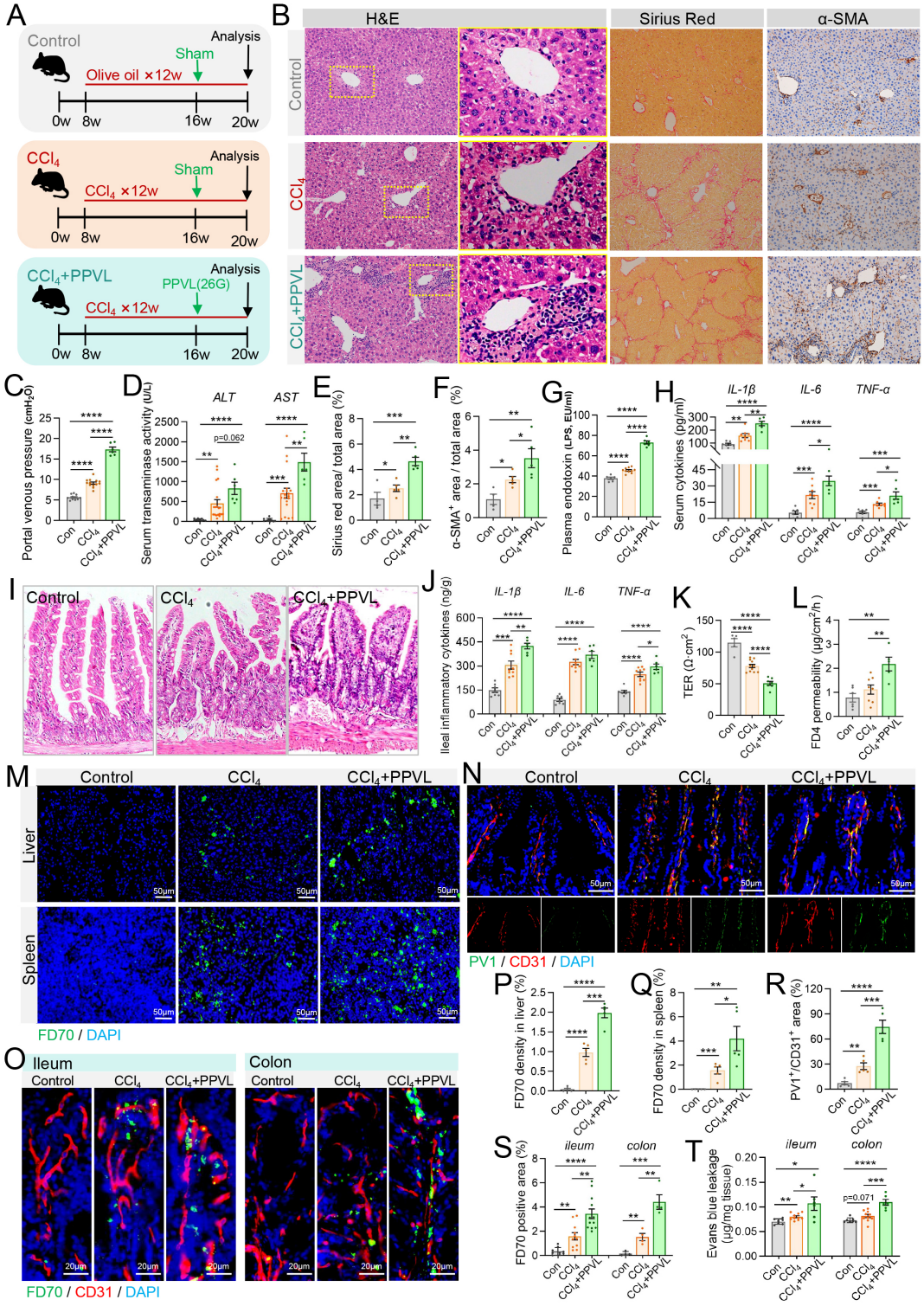


Figure 1

PH mediated GVB disruption promoted intestinal and systemic inflammation in CCl_4-induced liver cirrhosis. (A) Modeling and grouping scheme, including the control group (olive oil with sham operation), CCl_4 group (CCl_4 with sham operation) and CCl_4+PPVL group (CCl_4 with partial portal vein ligation). **(B)** Typical images of HE staining, Sirius red staining and immunohistochemical staining (α-SMA) of liver tissues. **(C)** Portal venous pressure measured via the water column method. n=6 to 12 for each group.

(D) Activity of serum alanine aminotransferase (ALT) and aspartate aminotransferase (AST). n=6 to 12 for each group. **(E-F)** The fibrosis ratio was calculated as the Sirius red^{+} and α-SMA^{+} area relative to total area. n=5 for each group. **(G-H)** Levels of plasma endotoxin and serum cytokines of IL-1β, IL-6 and TNF-α. n=6 to 8 for each group. **(I-J)** HE staining images and levels of inflammatory cytokines of IL-1β, IL-6 and TNF-α in ileal tissues. n=6 to 8 for each group. **(K-L)** Transepithelial resistance (TER) and FD4 permeability of intestinal mucosa detected by Ussing chamber. n=6 to 8 for each group. **(M, P-Q)** The FD70 density detected in the liver and spleen while was injected into the intestinal loop. n=5 for each group. **(N, R)** The PV1 expression on vascular endothelium in the ileum, and calculated as the PV1^{+}/CD31^{+} area. n=5 for each group. **(O, S)** The vascular leakage of FD70 into the ileal and colonic tissues while was injected from the tail vein. **(T)** The vascular leakage of Evans blue into the ileum and colon while was intravenous injected. n=6 to 10 for each group. $^{*}p<0.05$, $^{**}p<0.01$, $^{***}p<0.001$, $^{****}p<0.0001$.

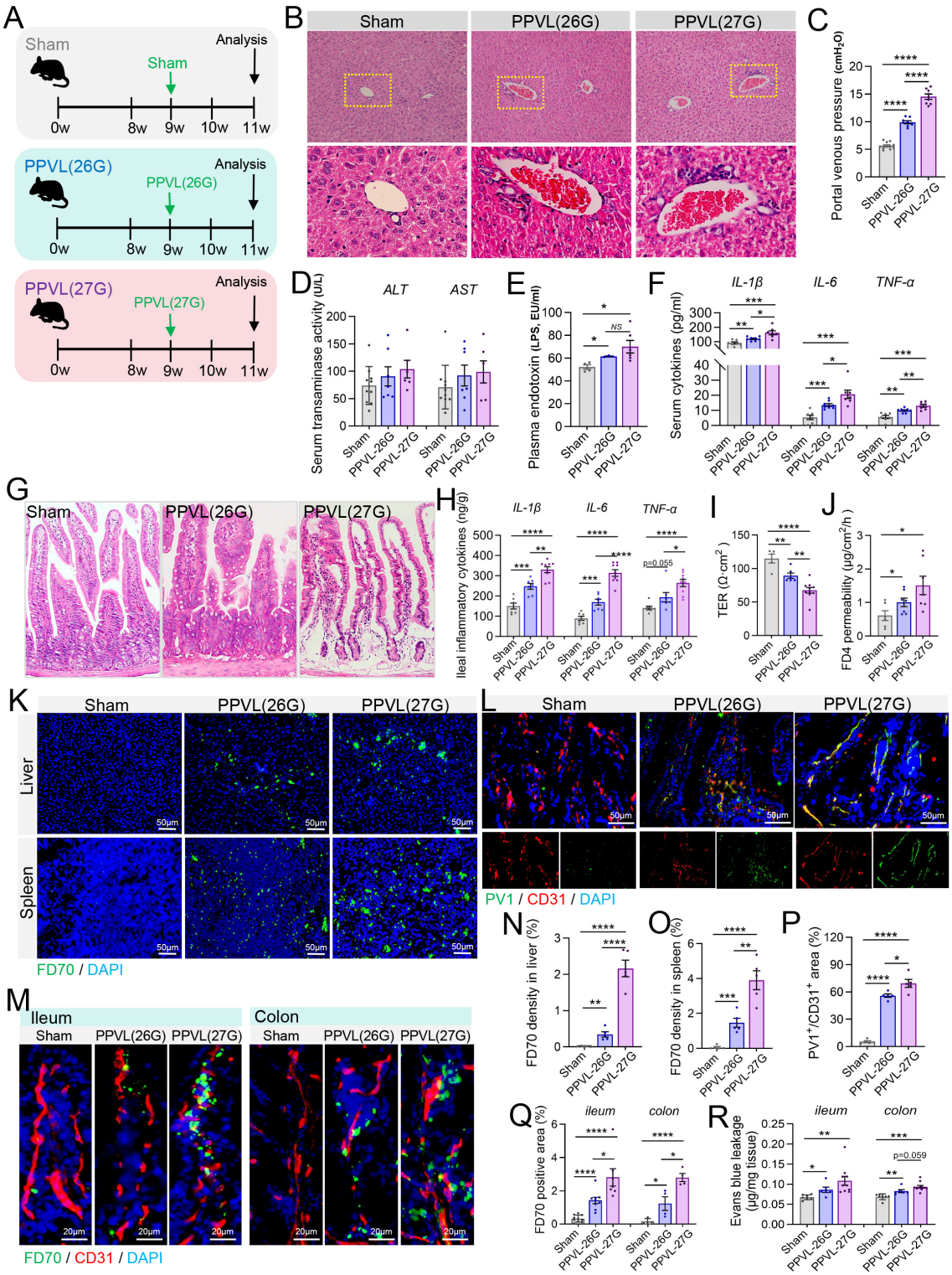


Figure 2

GVB collapse contributed to gut inflammation and leakage, and systemic injury in PPVL-induced prehepatic PH. (A) Modeling and grouping scheme, including the sham group (with sham operation), PPVL-26G group (ligation with a 26G needle) and PPVL-27G group (ligation with a 27G needle). **(B)** Typical images of HE staining of liver tissues. **(C)** Portal venous pressure measured via the water column method. n=8 to 10 for each group. **(D)** Activity of serum ALT and AST. n=8 to 10 for each group. **(E-F)**

Levels of plasma LPS and serum cytokines of IL-1β, IL-6 and TNF-α. n=6 to 8 for each group. **(G-H)** HE staining images and levels of inflammatory cytokines of IL-1β, IL-6 and TNF-α in ileal tissues. n=6 to 8 for each group. **(I-J)** Transepithelial resistance (TER) and FD4 permeability of intestinal mucosa detected by Ussing chamber. n=5 to 8 for each group. **(K, N-O)** The FD70 density detected in the liver and spleen while was injected into the intestinal loop. n=5 for each group. **(L, P)** The PV1 expression on vascular endothelium in the ileum, and calculated as the $PV1^{+}/CD31^{+}$ area. n=5 for each group. **(M, Q)** The vascular leakage of FD70 into the ileal and colonic tissues while was injected from the tail vein. **(R)** The vascular leakage of Evans blue into the ileum and colon while was intravenous injected. n=6 to 10 for each group. $^{*}p<0.05$, $^{**}p<0.01$, $^{***}p<0.001$, $^{****}p<0.0001$.

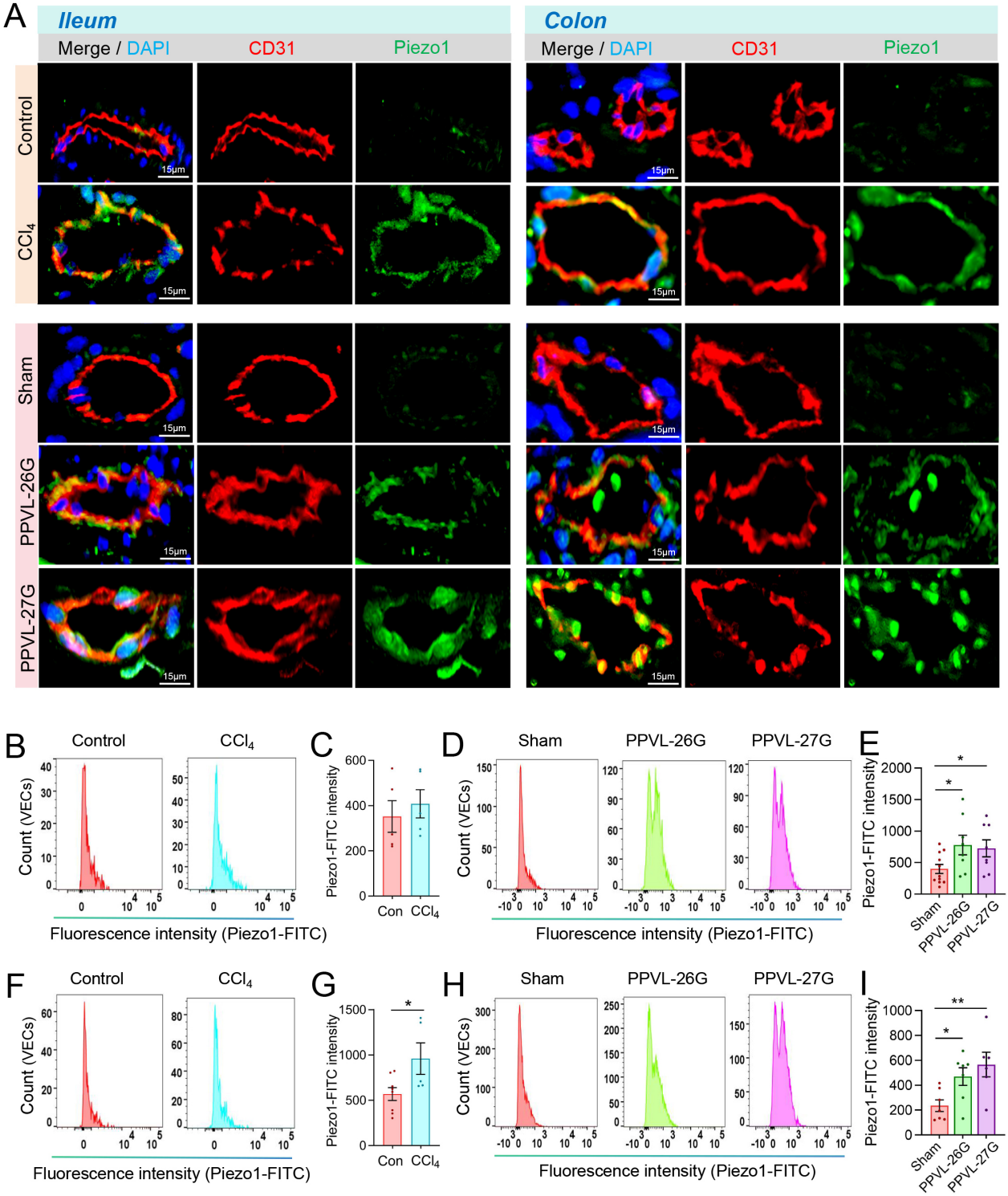


Figure 3

Upregulated Piezo1 in the intestinal microvascular ECs under portal hypertension of CCl_4 and PPVL Mice. (A) The expression intensity of Piezo1(green) in microvascular ECs (CD31, red) of the ileum (left panel) and colon (right panel) presented via immunofluorescence. DAPI (blue) displayed the cell nucleus. **(B-I)** The average expression of Piezo1 (fluorescence intensity of Piezo1-FITC) in $CD45^{-}CD90^{-}CD31^{+}$ vascular ECs in the ileum and colon via flow cytometry, namely, B-C for the ileum of the CCl_4 and control

mice, D-E for the ileum of the PPVL-26G, PPVL-27G and sham mice; while F-G for the colon of the CCl_4 and control mice, H-I for the colon of the PPVL-26G, PPVL-27G and sham mice. n=5 to 10 for each group. *p<0.05, **p<0.01.

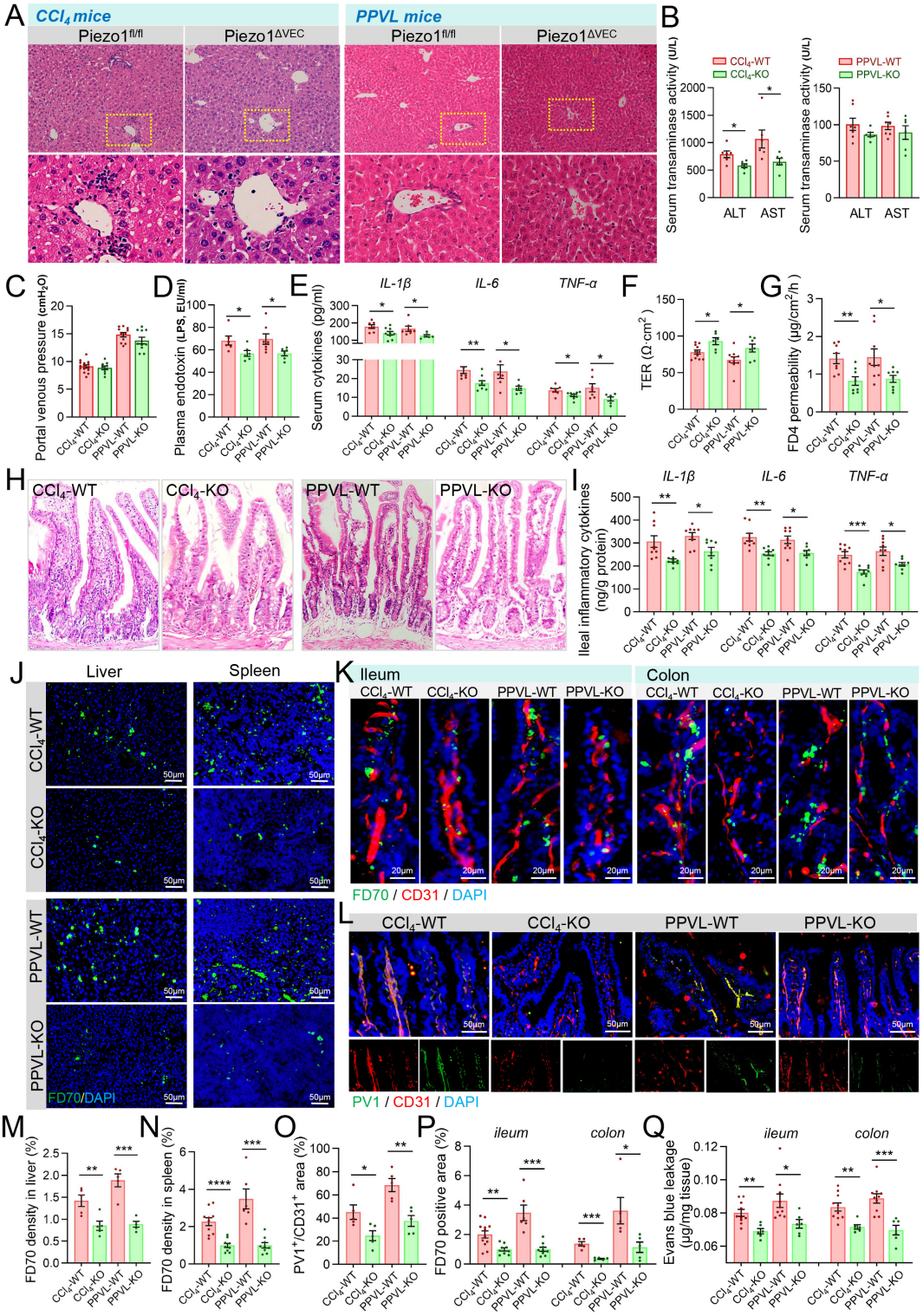


Figure 4

Endothelial Piezo1 knockout improved GVB dysfunction and leaky gut induced by PH in CCl_4 and PPVL mice. (A) Typical images of HE staining of liver tissues of the CCl_4 mice (left panel) and the PPVL mice (right panel) with a $Piezo1^{fl/fl}$ (WT) or $Piezo1^{\Delta EC}$ (KO) background. **(B)** Activity of serum ALT and AST. n=6 to 7 for each group. **(C)** Portal venous pressure in CCl_4 and PPVL mice with endothelial Piezo1 knockout. **(D-E)** Levels of plasma LPS and serum cytokines of IL-1β, IL-6 and TNF-α. n=6 to 10 for each group. **(F-G)** Transepithelial resistance (TER) and FD4 permeability of intestinal mucosa assessed by Ussing chamber. n=6 to 10 for each group. **(H-I)** HE staining images and levels of inflammatory cytokines of IL-1β, IL-6 and TNF-α in ileal tissues. n=8 to 10 for each group. **(J, M-N)** The FD70 density detected in the liver and spleen while was injected into the intestinal loop. **(L, O)** The PV1 expression on vascular endothelium in the ileum, and calculated as the $PV1^+/CD31^+$ area. n=5 for each group. **(K, P)** The vascular leakage of FD70 into the ileal and colonic tissues while was injected from the tail vein. **(Q)** The vascular leakage of Evans blue into the ileum and colon while was intravenous injected. n=6 to 10 for each group. $^*p<0.05$, $^{**}p<0.01$, $^{***}p<0.001$, $^{****}p<0.0001$.

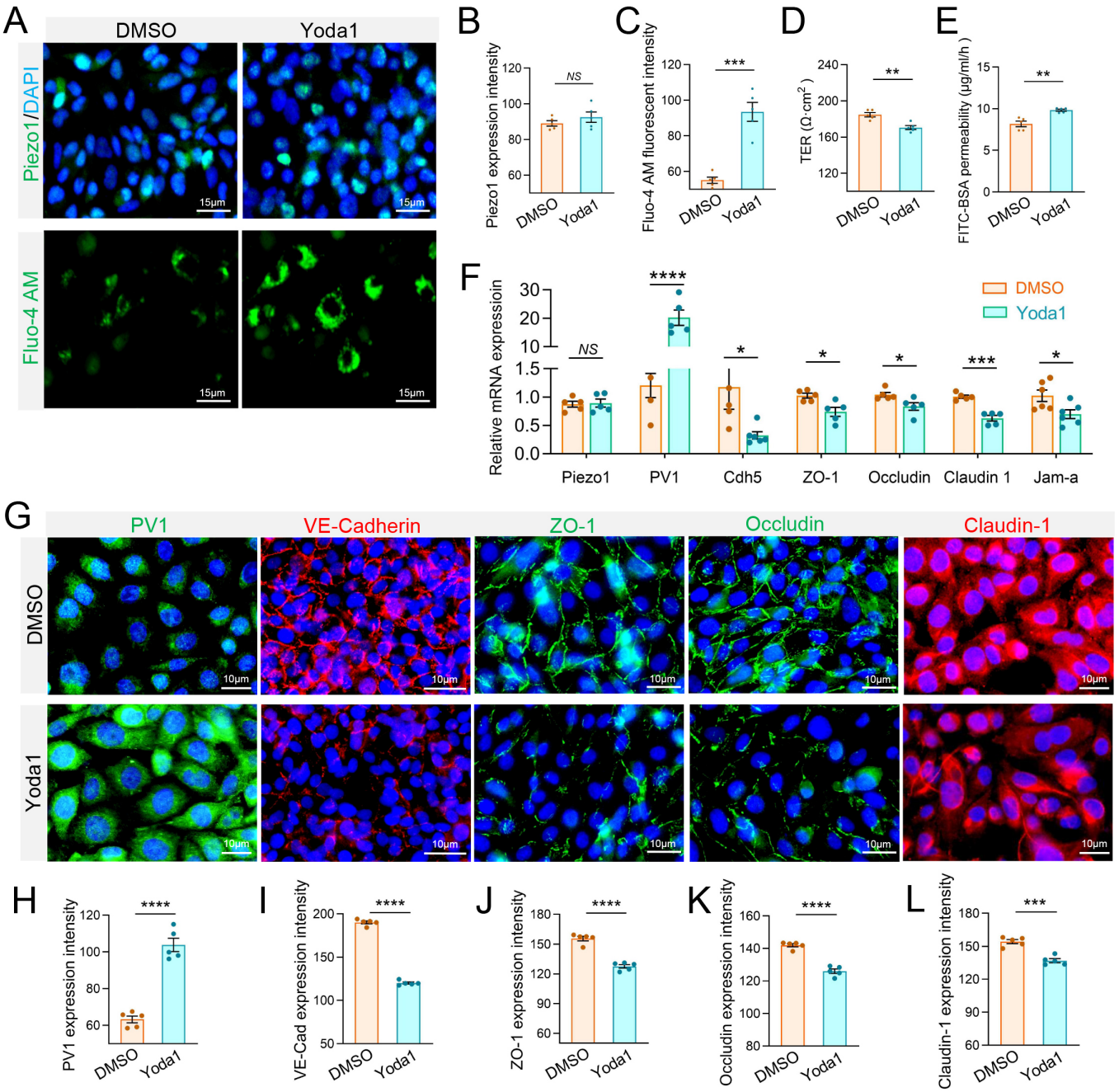


Figure 5

Piezo1 activation by Yoda1 triggered the increased permeability of intestinal microvascular ECs. (A-C) Yoda1 activated Piezo1 channel and triggered Ca^{2+} influx in intestinal microvascular ECs, with increased Fluo-4AM intensity but no significant changes in Piezo1 expression. **(D-E)** Increased permeability of endothelial barrier, with decreased transendothelial cell resistance (TER) and increased passage of macromolecular FITC-BSA, upon Piezo1 activation by Yoda1. **(F)** Yoda1 treatment increased the mRNA expression of PV1 and down-regulated the expression of junctional proteins in ECs. **(G-L)** The typical images and expression intensity of PV1, VE-cadherin, occludin, claudin-1, ZO-1 and JAM-A in ECs treated by Yoda1. n=5 to 6 for each group. $^{*}p<0.05$, $^{**}p<0.01$, $^{***}p<0.001$, $^{****}p<0.0001$.

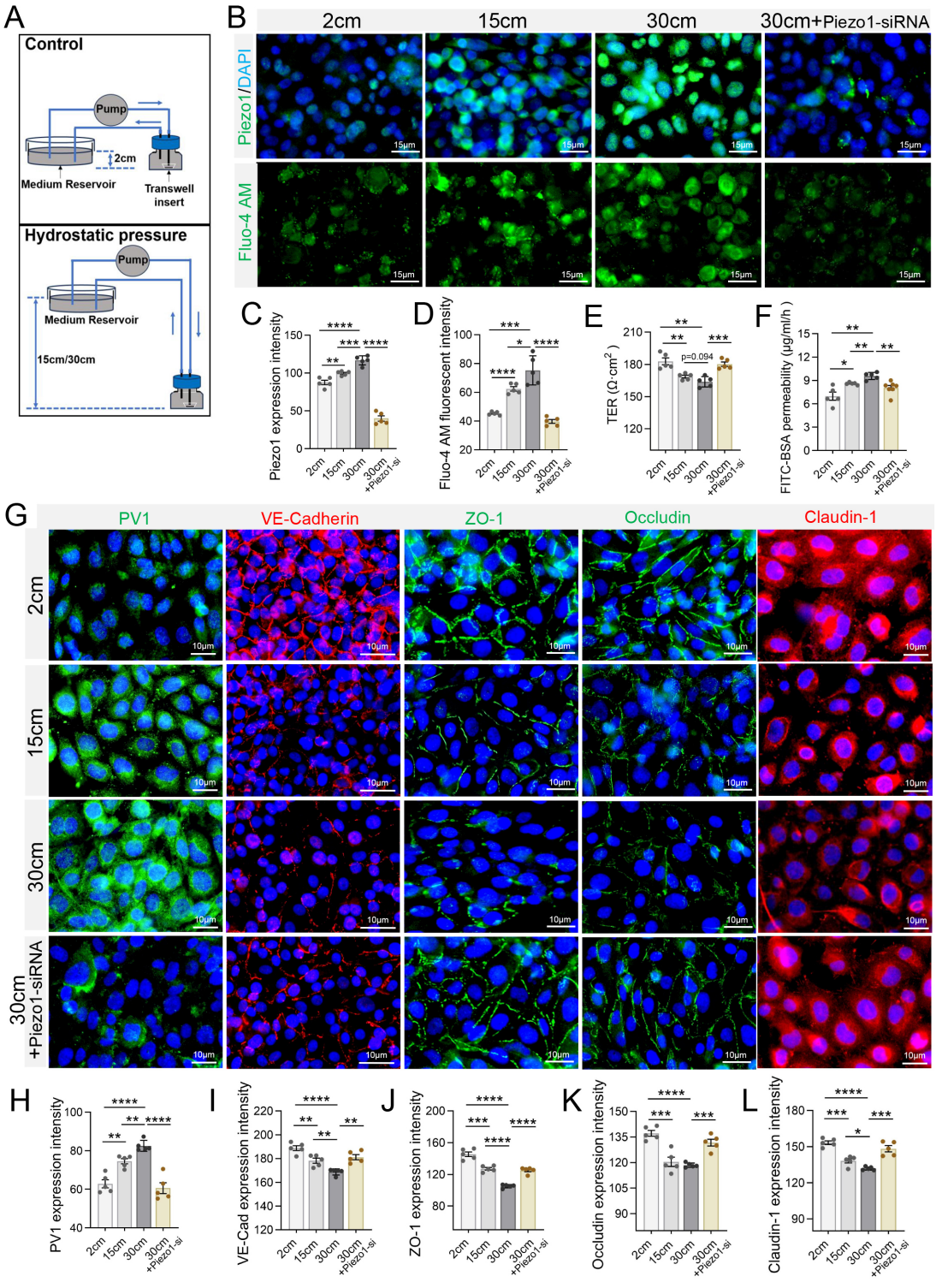


Figure 6

Hydrostatic pressure activated endothelial Piezo1 and promoted junctional damage and hyper-permeability of ECs. (A) The schematic diagram of experimental apparatus for hydrostatic pressure. The culture chamber (a closed culture bottle) was filled with medium, where the cell-planted transwell membrane or coverslip was placed. The height of the medium reservoir was adjusted to maintain the pressure in the culture (2cm, 15cm, 30cm). The medium in the culture chamber and the medium

reservoir was circulated by a peristaltic pump to ensure gas exchange and maintain stable oxygen tension. **(B-D)** The Piezo1 expression and intracellular Ca^{2+} concentration in ECs treated with hydrostatic pressure (2cm, 15cm, and 30cmH_2O), as well as in the condition of Piezo1 silence with specific siRNA. **(E-F)** Reduced TER and increased FITC-BSA permeability in ECs monolayer was shown as the hydrostatic pressure elevated, which could be blocked by Piezo1-siRNA. **(G-L)** The typical images and expression intensity of PV1, and junctional proteins including VE-cadherin, occludin, claudin-1, ZO-1 and JAM-A in ECs treated with hydrostatic pressure and Piezo1-siRNA. n=5 for each group; $^{*}p<0.05$, $^{**}p<0.01$, $^{***}p<0.001$, $^{****}p<0.0001$.

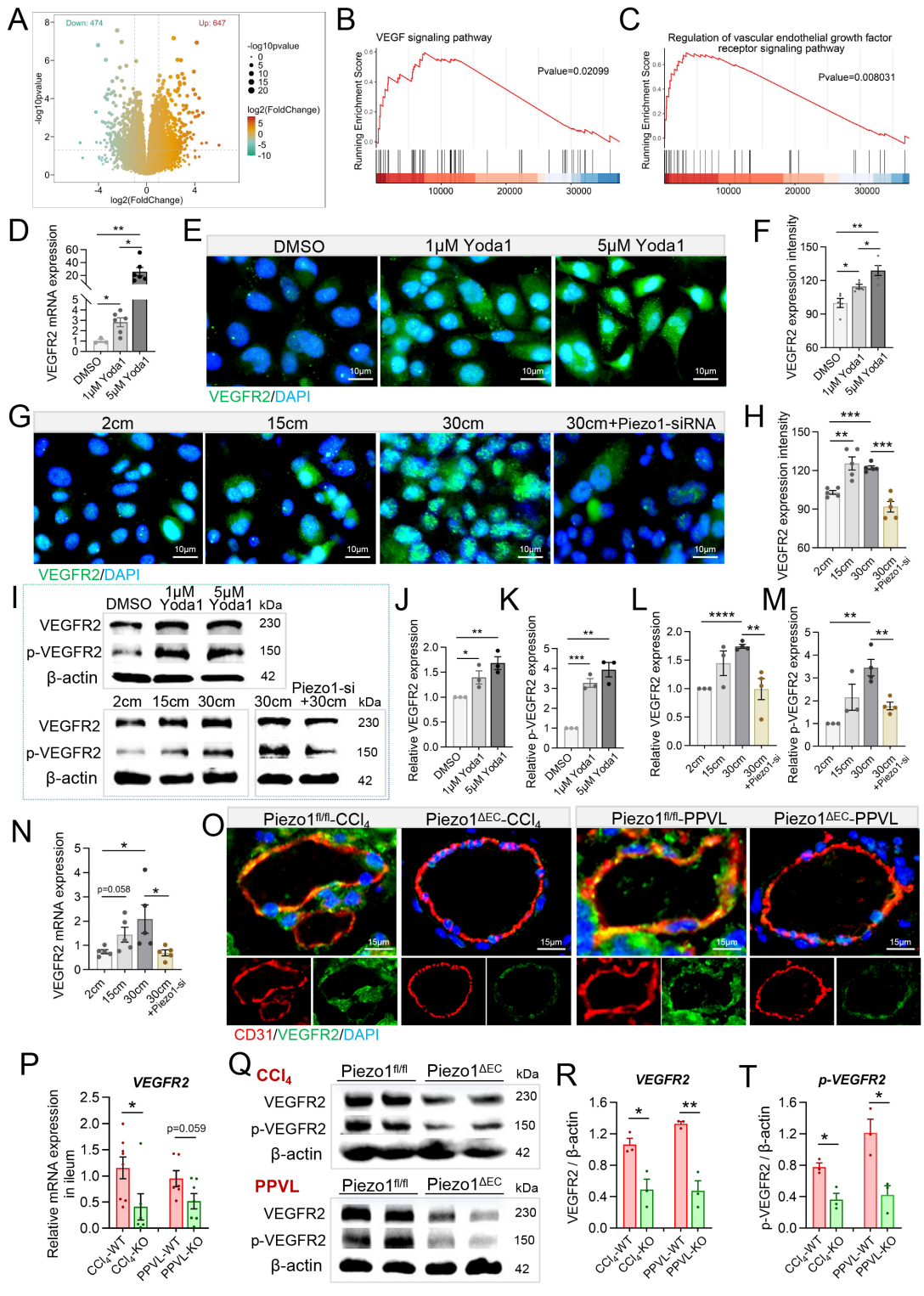


Figure 7

Piezo1 promoted endothelial hyperpermeability and GVB dysfunction via activating the VEGFR2 signaling. (A) The differential genes were identified and exhibited via volcano plot based on the RNA sequencing data, and **(B-C)** the GSEA analysis illustrated the enrichment of the VEGF signaling pathway and the VEGFR regulation pathway in ECs treated with 1μM Yoda1. n=4 for each group. **(D-F)** The expression of VEGFR2 in ECs treated with Yoda1 (1μM and 5μM) and DMSO quantified by RT-PCR and IF.

n=3 to 6 for each group. **(G-H, N)** The expression of VEGFR2 in ECs treated with hydrostatic pressure (15cm and 30cmH_2O) and preconditioned by Piezo1-siRNA detected by IF and RT-PCR. n=5 for each group. **(I-M)** The protein expression and phosphorylated level of VEGFR2 in ECs treated with Yoda1 or hydrostatic pressure detected by Western blot. n=3 to 4 for each group. **(O)** Typical images of VEGFR2 (green) expression in ileal vascular ECs (CD31, red) in CCl_4 and PPVL mice with a $Piezo1^{fl/fl}$ (WT) or $Piezo1^{\Delta EC}$ (KO) background. **(P)** The mRNA expression, and **(Q-T)** the protein expression and phosphorylated level of VEGFR2 in ileal tissues of CCl_4 and PPVL mice and those with endothelial Piezo1 KO. n=3 for each group. $^{*}p<0.05$, $^{**}p<0.01$, $^{***}p<0.001$, $^{****}p<0.0001$.

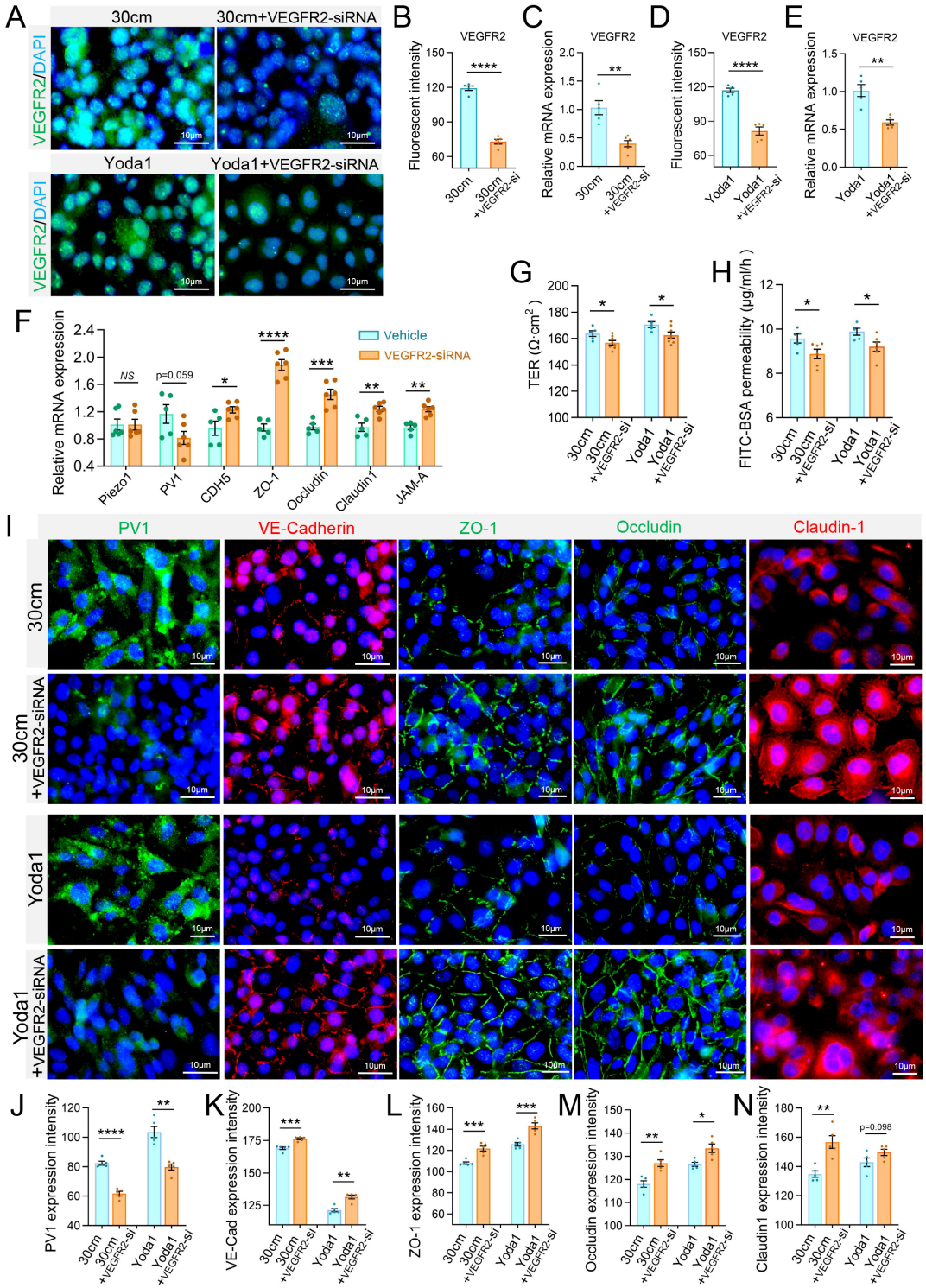


Figure 8

Silence of VEGFR2 alleviated Piezo1-mediated dysfunction and hyper-permeability of intestinal microvascular ECs. (A) ECs-model with silence of VEGFR2 was successfully established via specific siRNA, and **(B-E)** the mRNA and protein expression of VEGFR2 were markedly inhibited by siRNA in ECs treated with hydrostatic pressure and Yoda1, detected by IF and RT-PCR. **(F)** VEGFR2 knockdown by siRNA improved the mRNA expression of PV1 and junctional proteins induced by Piezo1 activation in

ECs, and **(G-H)** ameliorated the dysfunction of endothelial barrier induced by Yoda1 (5μM) or hydrostatic pressure (30cmH_2O), with increased TER and decreased FITC-BSA permeability. **(I-N)** The typical images and expression intensity of PV1, VE-cadherin, occludin, claudin-1, ZO-1 and JAM-A in ECs treated with hydrostatic pressure and Yoda1, as well as VEGFR2-siRNA. n=5 to 6 for each group. $^{*}p<0.05$, $^{**}p<0.01$, $^{***}p<0.001$, $^{****}p<0.0001$.

Supplementary Files

This is a list of supplementary files associated with this preprint. Click to download.

- TableS1.docx
- TableS2.docx
- SupplementaryMethods.docx
- Graphicalabstract.gif
- SupplementaryFigures.docx
- SupplementaryMethods.docx
- Supplementarymaterial.docx